Investigating the gelation mechanism of a colloid gel with thermo-reversible color change using SANS

Yun Liu, Elizabeth G. Kelley, Susana C. Marujo Teixeira

2026 Neutron School on Small Angle Neutron Scattering and Neutron Reflectometry

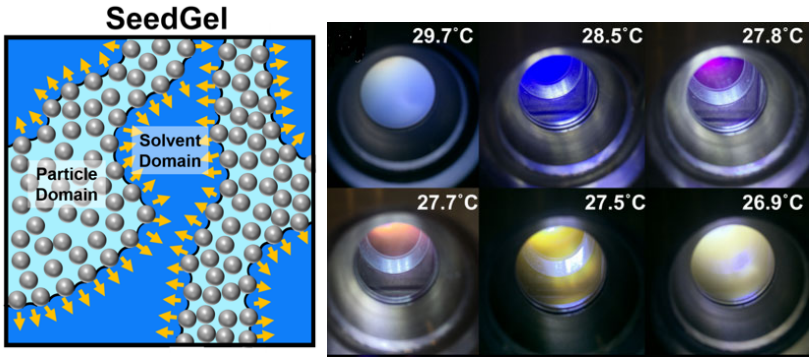

Abstract

Small Angle Neutron Scattering (SANS) probes structures over length scales from about one nanometer to hundreds of nanometers and is widely used for soft-matter systems. In this neutron school experiment, we study a new class of colloidal gels formed in binary solvents, known as solvent-segregation-driven gels (SeedGels).[1] When colloidal particles are dispersed in a binary solvent with one solvent component preferentially attracted to the particle surfaces, the microscopic solvent phase separation can lead to the formation of a SeedGel with colloidal particles to preferentially jam within one solvent phase, creating distinct particle-rich and solvent-rich domains. SeedGels are thermoreversible and exhibit highly reproducible structures upon temperature cycling. Some systems also show temperature-controlled, tunable coloration across the visible spectrum, enabling potential optical applications.[2] By measuring samples as a function of temperature and using contrast variation, SANS provides insight into the gelation mechanisms of SeedGels. Various aspects of the experiments from the sample preparation and SANS instrument setup to data treatment and interpretation will be discussed.

1. Introduction to colloidal particles in binary solvents

Colloidal systems consist of particles dispersed in a solvent with the size typically ranging from about one nanometer to about a couple of micrometers. The motions of particles are mostly driven by Brownian motions and the gravity typically does not play an important role for their mobility. These colloidal systems are commonly encountered in our everyday life, such as therapeutic drugs, paints, and shampoos.

The phase behavior of colloidal particle is determined by the effective interaction between these colloidal particles. If the interaction is dominatingly repulsive, particles tend to be away from each other so that they are stable in solutions even at fairly high particle concentrations. If the interaction is attractive, particles like to aggregate to form large clusters, cause phase separation, or become a solid gel. This inter-particle interaction is influenced by both the direct interactions between particles, such as hard sphere interactions, and also the solvent molecules, such as counter ions, co-ions, and solvent fluctuations. The phase behavior of particles in a real system is equivalent to the phase behavior of colloidal particles interacting with this effective interaction potential. The effective interaction potential is considered as a coarse-graining method to simplify our way to investigate the structure and phase behavior of particles in a real system.

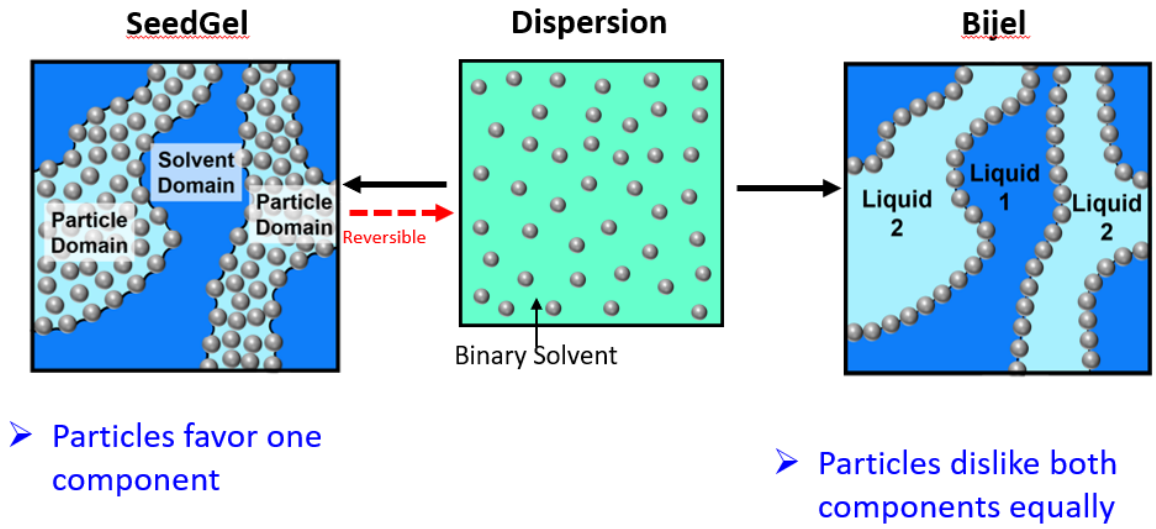

Figure 1. The schematic figures of SeedGel and Bijel to show the different structures of particles in a SeedGel and Bijel samples. Both types of gels are formed by dispersing particles in a binary solvent. Depending on the surface properties of a sample, a sample can become either a Bijel or a SeedGel by changing the sample temperature.

For particles dispersed in a binary solvent, the effective inter-particle interaction depends on the particle surface properties as well as the binary solvent. A binary solvent is made of two types of solvent molecules that are partially miscible with each other. In 1978, Fisher and de Gennes showed that when the binary solvent condition moves closer to its critical point, there is an

effective attraction generated between particles due to the long range solvent fluctuation.[3] This critical phenomenon induced attraction was also called critical Casmir forces,[4] and was found to be responsible for the aggregation behavior of silica particles dissolved in a binary solvent.[5] And when the attraction strength is strong enough, the particles can form a gel. By tuning the surface of particles strongly favored by one component of the binary solvent, it has been recently demonstrated that a system can form a special type of colloidal gel, which is termed as SeedGel as shown in Figure 1.[1] During the gel formation, the binary solvent is also phase separated into two different liquid regions, shown as "1" and "2" in Figure 1. Each region is only rich for one type of molecules in a binary solvent. Note that if the surfaces of particles dislike both components of the binary solvent, it can form a Bijel as also illustrated in Figure 1.[6,7] For SeedGel, there is the phase separation of particles as well as the binary solvent. Since particles like one component of the binary solvent, all particles are jammed into one liquid/solvent region to form particle domain. The other liquid/solvent region, consisting of mainly the solvent component the particles dislike, forms the solvent domain.[1] Note that in a Bijel system, when the solvent phase separates, particles stay at the interface of the two solvent domains. One can consider that SeedGel and Bijel are two extreme cases for colloidal particles dissolved in a binary solvent. In this experiment, we plan to study the structures of a model SeedGel system: charged silica particles dissolved in a typical binary solvent, water/2,6-lutidine.

2. A model SeedGel system: charged silica particles in water/2,6-lutidine

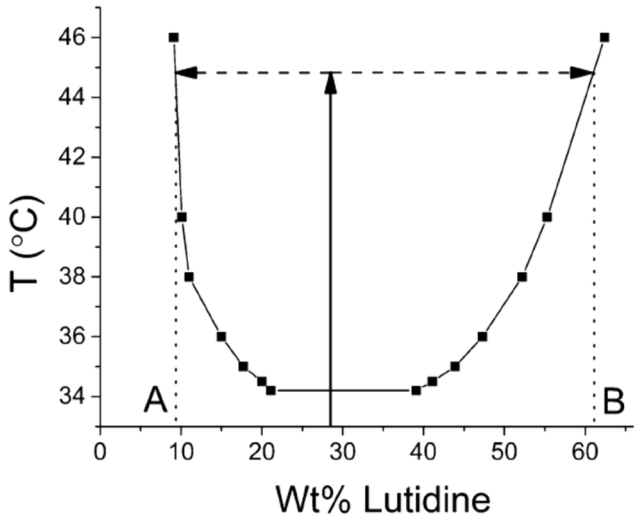

Figure 2. It shows the phase diagram of a binary solvent, water/2,6-lutdidine. Water and 2,6-lutidine are miscible at low temperatures. However, when increasing the temperature above the demixing line (solid line), water and lutidine become phase separated. The critical temperature of this binary solvent is around 34 ºC.

Figure 2 shows the phase behavior of the binary solvent with water and 2,6-lutidine, which is a lower critical solution temperature (LCST) system. The critical concentration for lutidine is about 29 % mass fraction with the critical temperature at about around 34 ºC for H_2O/lutidine.[8] Replacing H_2O with D_2O can decrease the critical temperature by a couple of degrees. At low temperature, water and 2,6-lutidine are fully miscible for any given relative concentrations of lutidine and water. When increasing the temperature, it becomes less soluble. Once crossing the demixing temperature, the bulk solvent becomes phase separated with two phases: one liquid phase is rich in water and another liquid phase is rich in lutidine. To prepare a sample to form a SeedGel, charged silica particles, whose diameter is about 27 nm, are added in the solvent with water/lutidine. Water in the binary solvent is preferentially adsorbed on the surface of the silica particles.[9] For the sample studied in this summer school experiment, the volume fractions for particles, water, and lutidine in this sample are about 24 %, 53%, and 23% respectively. Because charged silica particles really like water, when heating the sample, it can form a SeedGel by increasing the temperature.

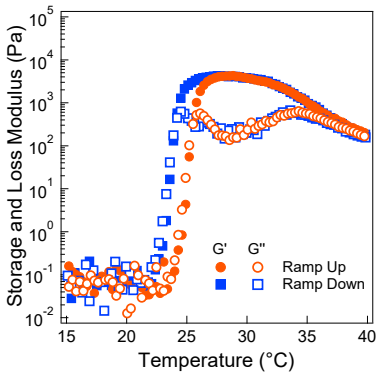

Figure 3. (a) Rheological behavior of the sample as a function of the temperature.

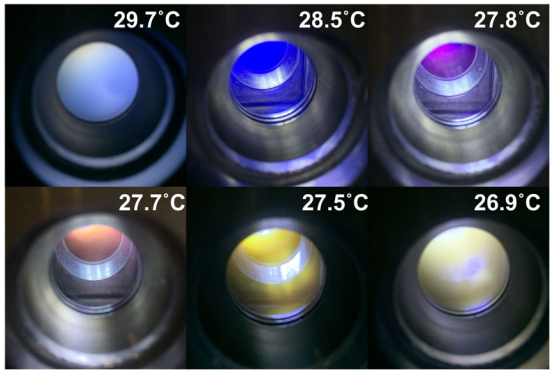

Figure 4. This SeedGel samaple shows different colors when there is a white light scoure behind the sample.

Figure 3 shows the storage (G') and loss (G") modulus of this sample at different temperatures.[10] At room temperature, the sample remains as a transparent liquid sample and both moduli are very small. However, when heating the sample, it becomes a solid gel at the temperatere from around 26 ºC to 34 ºC as G' becomes larger than G" within this temperature range. The question is how we can prove that the sample indeed becomes a SeedGel at this temperature range, which will be answer by the expeirment in this neutron school.

And very interestingly, as shown by Figure 4, the sample shows different colors at differenent temperatures when putting a whilte light source behind of the sample.[2] The color of the sample is reversibly adjustable by changing the sample temperature. All individual components of the sample (water, lutidine, and silica paritcles) do not show any color effect withint this temperature range. At low temperaature when the sample is liquid, the sample is transparent. Thus, the color effect of this SeedGel sample is driven by the structures formed in the SeedGel. It is thus very important to study the structures as a function of the tempearture and understand the strucutral origin of the color.

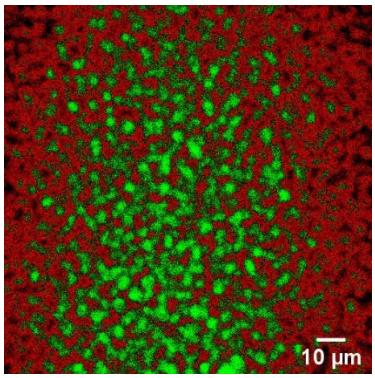

Figure 5. Confocal image of a SeedGel sample by adding dye molecules.

Preliminary confocal image of the SeedGel sample shows that the particles form a bicontinuous structures with the channel size at micrometer level.[1] But a confocal microscopy cannot measure the structure at smaller length scale. Therefore, we will use SANS to investigate the structures of this model SeedGel system.

<u>To summary the questions we hope to answer:</u>

SANS is a powerful tool to study structures of colloidal gels. A couple of key questions we hope to resolve using SANS are

- To prove that the colloidal gel is a SeedGel, we need to show experimentally that the binary solvent is also phase separated into two domain commensurate with the particle domains. SANS is only tool to answer this question.
- To understand the temperature dependence of the elastic modulus, it is important to probe the structure of colloidal particles at the liquid and gel state.

- Through SANS experiment, we want to know what is the structural origin of the sample color.

3. Prepare your experiment

3.1. Choose the right instrument

We need to measure over a range of angles spanning two orders of magnitude in q and an appropriate
q-spacing at low q-values. For the neutron scattering experiments, the Q range of the instrument determines the length scale it can probe.

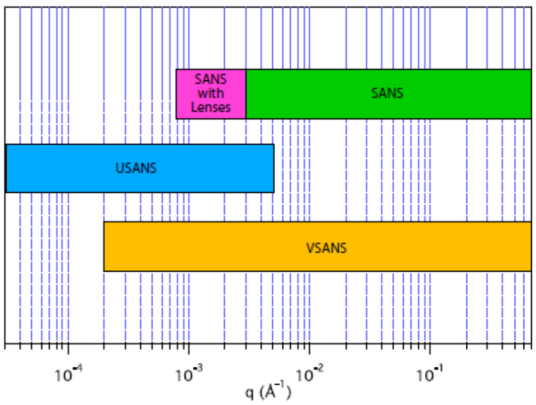

Figure 6**:** Comparison of the accessible q ranges of the BT-5 USANS instrument, NG-3 and NG-7 SANS instruments and the VSANS instrument currently under construction.

Figure 6 shows the Q range covered by different instruments. To probe the colloidal particle arrangements with the diameter around 27 nm, we hope to reach Q value around 0.02 $Å^{-1}$. When particles form clusters, the cluster size becomes big that needs smaller Q value. Therefore, both vSANS and SANS with lens should be ok for our experiments. However, to probe the domain structure with the length scale on the order of a few micrometers as shown in Figure 5, it needs Q range around 10^{-4} $Å^{-1}$, which is only accessible by using USANS. Therefore, to fully characterize our SeedGel samples, we should request two instruments: one is SANS or vSANS; another one is USANS. In this experiment, we focus on understand the structures of particle packing, which needs the Q range provided by SANS/vSANS. The following experiment was done using SANS with lens.

3.2 Understand the basics of a SANS instrument

A schematic of the 30-m SANS instrument is shown in Figure 7. The instrument configuration parameters, and their allowed range for the NGB 30m SANS, are listed in Table1. In order to determine the instrument configurations, we will use the SASCALC tool available at NCNR.

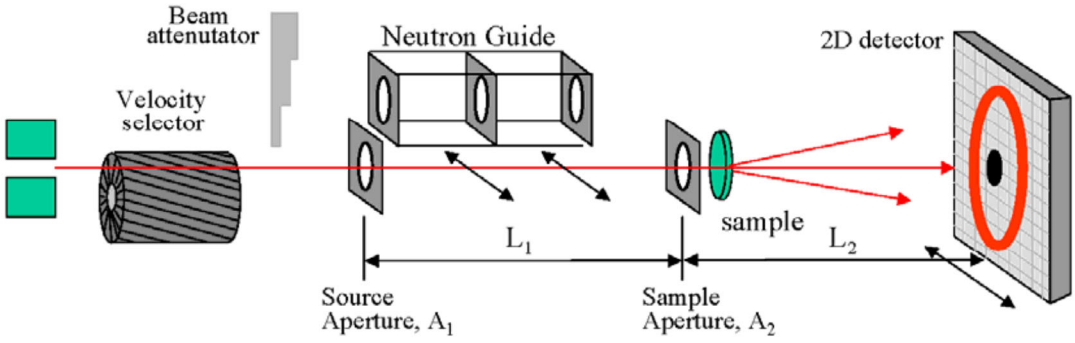

Figure 7. Schematic diagram of the components of the NCNR's 30-m SANS instruments.

Table 1. Instrument configuration parameters and their range of allowed values for the NGB 30-m SANS instrument.

Variable	**Allowed values**
Neutron wavelength	*3-20 Å (determined by rotational speed of the velocity selector)*
Wavelength spread (FWHM)	*0.10 to 0.3 (determined by the spinning frequency and inclination of the velocity selector)*
Number of neutron guides	0-8 (determines the beam collimation by changing the distance of the source aperture from the sample)
Source aperture diameter	1.43, 2.54, or 3.81 cm for 0; 5.0 cm for 1-8 guides
Sample-to-detector distance	133-1317 cm
Detector offset	*0-25 cm (detector translation perpendicular to beam to extend the q-range covered at a given distance)*
Sample aperture diameter	*0-2.5cm*
Beamstop diameter	*2.54, 5.08, 7.62, or 10.16 cm*
Beam attenuator	10 choices of beam attenuator thickness to reduce beam intensity for sample transmission measurements

4.2. Plan the SANS configurations using SASCALC

For a given set of allowed parameters, SASCALC computes the corresponding q-range and the beam intensity (n/sec) on the sample. q is the magnitude of the scattering vector, which can be calculated as $q = |\vec{q}| = \frac{4\pi}{\lambda}\sin(\frac{\theta}{2})$ for elastically dominating scattering events. λ and θ are neutron wave length and scattering angle, respectively. The q-range for a particular configuration is determined by the choice of wavelength, detector distance and detector offset. A wavelength of 6 Å is typical for most SANS measurements at NCNR. A wavelength spread of $\Delta\lambda/\lambda$ of 0.11 is typical on SANS instruments as it provides an adequate balance of flux and q-resolution. In general, we choose the largest number of neutron guides (allowed in the desired q-range) in order to maximize the beam intensity on the sample.

There are several considerations that must be taken into account when determining instrument configurations for SANS measurement. For the short distance, the detector can cover a wide range of q due to its capability to measure scattered neutrons at large angles. For this distance, we usually put as many neutron guides in as possible.

To reach low-q, the detector needs to be far away from the sample as possible. For this long detector distance, we are interested in low-q range. Therefore, the beam divergence caused by the neutron guides becomes the limiting factors determining its low-q limit. Hence, at the long detector distance, we typically put less neutron guides in.

After having the configurations at both short and long detector distance, the q range covered by the two configurations sometimes may not overlap with a gap for some q range. Therefore, it is common to have a configuration at the intermediate distance so that the full q range accessible by the instrument can be covered.

All that remains is to select a combination of sample-to-detector distances and detector offsets that will yield the appropriate q -range for our measurements. For the high-q limit of the instrument, we will use the shortest sample-to detector distance, 133 cm, and the maximum detector offset, 25 cm. We will choose 8 guides at this distance to maximize the neutron flux. The results from SASCALC for these choices are as follows:

Source Aperture Diameter = 5.00 cm
Source to Sample = 387 cm
Sample Aperture to Detector = 138 cm
Beam diameter = 3.68 cm
Beamstop diameter = 2.00 inches
Minimum Q-value = 0.0304 1/ Å (sigQ/Q = 17.5 %)
Maximum Horizontal Q-value = 0.4211 1/ Å
Maximum Vertical Q-value = 0.2467 1/ Å
Maximum Q-value = 0.4742 1/ Å (sigQ/Q = 5.2 %)
Beam Intensity = 6094620 counts/s
Figure of Merit = 2.19e+08 Å ^2/s
Attenuator transmission = 0.000285 = Atten # 8
********** CGB *** CGB **********
Sample Aperture Diameter = 1.27 cm
Number of Guides = 8
Sample Chamber to Detector = 133.0 cm
Sample Position is Chamber
Detector Offset = 25.0 cm
Neutron Wavelength = 6.00 Å
Wavelength Spread, FWHM = 0.125
Sample Aperture to Sample Position = 5.00 cm
Lenses are OUT

For the low-q limit of the instrument, we will use 8.09 Å to take advantage of the focusing lens at NGB 30m SANS to reach the smallest Q value possible (about 0.001 $Å^{-1}$). The detector has to be

at the longest sample-to detector distance, 1530 cm. The results from SASCALC for these choices are as follows:

Source Aperture Diameter = 1.43 cm
Source to Sample = 1627 cm
Sample Aperture to Detector = 1322 cm
Beam diameter = 1.43 cm
Beamstop diameter = 1.00 inches
Minimum Q-value = 0.0010 1/ Å (sigQ/Q = 38.5 %)
Maximum Horizontal Q-value = 0.0324 1/ Å
Maximum Vertical Q-value = 0.0182 1/ Å
Maximum Q-value = 0.0371 1/ Å (sigQ/Q = 5.2 %)
Beam Intensity = 20642 counts/s
Figure of Merit = 1.46e+06 Å ^2/s
Attenuator transmission = 0.0269 = Atten # 4
********** CGB *** CGB **********
Sample Aperture Diameter = 1.27 cm
Number of Guides = 0
Sample Chamber to Detector = 1317.0 cm
Sample Position is Chamber
Detector Offset = 25.0 cm
Neutron Wavelength = 8.40 Å
Wavelength Spread, FWHM = 0.125
Sample Aperture to Sample Position = 5.00 cm
Lenses are IN

For intermediate q -values, we wish to choose a detector distance such that it covers the gap between the q-range of the previous two configurations. After experimenting with a few values of the detector distance in SASCALC, we find that a detector distance of 400 cm with no offset will achieve our objective. We will choose 5 guides to maximize the count rate on the detector. The results from SASCALC for these choices are as follows:

Source Aperture Diameter = 5.00 cm
Source to Sample = 852 cm
Sample Aperture to Detector = 405 cm
Beam diameter = 4.46 cm
Beamstop diameter = 2.00 inches
Minimum Q-value = 0.0086 1/ Å (sigQ/Q = 24.6 %)
Maximum Horizontal Q-value = 0.0836 1/ Å
Maximum Vertical Q-value = 0.0836 1/ Å
Maximum Q-value = 0.1179 1/ Å (sigQ/Q = 5.4 %)
Beam Intensity = 1640200 counts/s
Figure of Merit = 5.9e+07 Å ^2/s
Attenuator transmission = 0.00141 = Atten # 8
********** CGB *** CGB **********
Sample Aperture Diameter = 1.27 cm

Number of Guides = 5
Sample Chamber to Detector = 400.0 cm
Sample Position is Chamber
Detector Offset = 0.0 cm
Neutron Wavelength = 6.00 Å
Wavelength Spread, FWHM = 0.125
Sample Aperture to Sample Position = 5.00 cm
Lenses are OUT

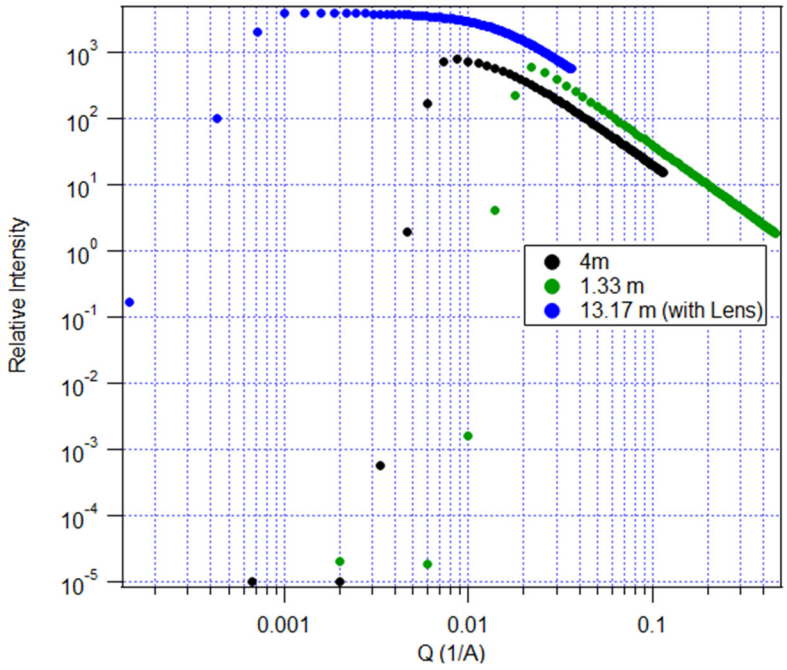

Figure 8. The q range covered by 3 configurations.

4. Setting up experiments and collecting data on SANS

Given the stated objectives of the experiment and knowledge of the instrument, how do we prepare the experiment to maximize our chances of scientific success? Here we discuss some of the issues that are worth considering before an experiment.

4.1. Scattering Contrast

In order to have enough scattering intensity, there must be scattering contrast. The absolute intensity of the neutron scattering can be expressed as $I(Q) = \phi V \Delta\rho^2 P(Q) S(Q)$ for monodispersed spherical particles. Hence, the scattering is proportional to the scattering contrast, $\Delta\rho$, where

$\Delta\rho = \rho_1 - \rho_2$ ← Scattering Contrast (2)

and ρ_1 and ρ_2 are the scattering length densities (SLD) of the particles and the solvent, respectively.

The scattering intensity is still proportional to $\Delta\rho^2$. And the contrast is the SLD of the two domains in the sample.

The SLD can be calculated using $\rho = \frac{\sum_{i=1}^{n} b_i}{V}$ (3)

where V is the volume containing *n* atoms, and b_i is the (bound coherent) **scattering length** of the i^{th} atom in the volume V. V is usually the molecular or molar volume for a homogenous phase in the system of interest.

The SLD of each component can be calculated from the above formula, using a table of the scattering lengths of elements. (The scattering length of different elements can be found at the NCNR website: https://www.ncnr.nist.gov/resources/n-lengths/.) It can be calculated using the interactive *SLD Calculator* at the NCNR's Web pages (http://www.ncnr.nist.gov/resources/index.html). In SANS experiments it is a common practice to deuterate one or more components to increase the contrast for the component under study. In particular, deuterating the solvent removes much of the incoherent background from the hydrogen, which is a limiting factor for many samples for measurements at high q (above 0.2 $Å^{-1}$), but this is not relevant for the USANS experiment.

Material	Chemical Formula	Mass Density (g/cc)	SLD (cm^{-2})
Water	H_2O	1.0	-0.56×10^{10}
Heavy water	D_2O	1.1	6.33×10^{10}
Silica particle	SiO_2	2.2	3.475×10^{10}
lutidine	C_7H_9N	0.925	1.156×10^{10}

Table 1. The scattering length densities (SLD) for the components used in this experiment.

Our sample has three components: H_2O, silica particles, and lutidine. The SLD of lutidine and H_2O is close to each other and the SLD of SiO_2 is much larger. The scattering data are expected dominated by the structures due to silica particles in the sample.

4.2. Sample Thickness

H**ow thick should one sample be?** The scattered intensity is proportional to the product of the sample thickness, d_s and the sample transmission, T. It can be shown that the transmission, which is the ratio of the transmitted beam intensity to the incident beam intensity, is given by

$$T = e^{-\Sigma_t d_d}, \quad (4)$$

where $\Sigma_t = \Sigma_c + \Sigma_i + \Sigma_a$, i.e. the sum of the coherent, incoherent and absorption macroscopic cross sections. The absorption cross section, Σ_a, can be accurately calculated from tabulated absorption cross sections of the elements (and isotopes) if the mass density and chemical compositions of the sample are known. The incoherent cross section, Σ_i, can be estimated from the cross-section tables for the elements as well. The coherent cross section, Σ_c, can only be estimated since it depends on the details of the structure of the atoms in the sample. This should be no surprise as Σ_c as a function of angle is the quantity we are aiming to measure! The scattered intensity is proportional to $d_s T$ and hence

$$I_{meas} \propto d_s e^{-\Sigma_t d_d} \quad (5)$$

which has a maximum at $d_s = 1/\Sigma_t$ which implies an optimum transmission, $T_{opt} = 1/e \approx 0.37$. The sample thickness at which this occurs is known as the "1/e-length". The NCNR web based SLD calculator provides estimates of Σ_i and Σ_a and gives an estimate of the 1/e-length as well as calculating the SLD.

4.3 Counting statistics

Counting statistics of a SANS experiment follows the Poisson distribution. The uncertainty, or more precisely the standard deviation, σ, for the number of counts, $I(t)$, is $\sigma \sim \sqrt{I(t)}$. For example, if the accumulated counts are 1000 counts per data point, its standard deviation is $\sqrt{1000} \sim 30$. Hence, a relative uncertainty of about 3 %.

A related question is how long the background and empty cell measurements should be relative to the sample measurement. The same $\sigma \sim \sqrt{I(t)}$ relationship leads to the following approximate result for the optimal relative counting times

$$\frac{t_{background}}{t_{sample}} \sim \sqrt{\frac{Count\ Rate_{background}}{Count\ Rate_{sample}}}$$

Hence if the scattering from the sample is weak, the background should be counted for as long (but no longer!) as the sample scattering. However, if the sample scattering count rate is, say, 4 times greater than the background rate, the background should be counting only half as long as the sample scattering.

5. Data reduction

What is needed to be collected in order to have the absolute scattering of your samples?

SANS collect the scattered neutrons as a function of scattering angle. When elastic scattering dominates (which is the case for SANS), it is equivalent to state that SANS collect the scattered

neutrons as a function of Q. The counting rate at different Q needs to be corrected for many instrument related factors, such as background, so that it reports the so called absolute intensity that is the differential macroscopic scattering cross section.

Ideally, the absolute intensity should be a value that only depends on the scattering of your samples, and independent of SANS instruments used to collect the data. However, the instrument resolution still affects the data. In order to finally obtain the absolute value, certain data have to be collected to correct the background scattering and other instrument factors.

In general, scattering intensity (neutron counts) recorded by the detector with the sample in the beam can come from 3 sources: 1) neutrons scattered by the sample itself (the scattering we are interested in); 2) neutrons scattered from something other than the sample, but pass through the sample; and 3) everything else, including neutrons that reach the detector without passing through the sample (stray neutrons or so-called room background) and electronic noise in the detector itself. To separate these three contributions, we need three measurements:

i) Scattering measured with the sample in place contains contribution from all 3 sources listed above, and is denoted as $\boldsymbol{I_{sam}}$.
ii) Scattering measured with empty cell (no sample in the cell) contains contributions from the 2nd and 3rd sources listed above, and is denoted $\boldsymbol{I_{emp}}$. This data is usually collected only once for an experiment as the scattering of the empty cell is usually considered the same for different samples.
iii) Counts measured with a complete absorber ("blocked beam") at the sample position contains only the contribution from the 3rd source listed above, and is denoted $\boldsymbol{I_{bgd}}$. This measurement is usually measured only once for an experiment as this background signal usually does not change with time.

In addition to the above three measurements, the transmission (the fraction of the incident beam intensity that passes through the sample without being scattered or absorbed) of the sample and the sample cell must also be measured in order to correctly subtract the contributions to the background and to calibrate the scattering on an absolute cross section scale.

5.1 Data reduction procedures

Data reduction is the process to convert the counting number at different scattering angles into the absolute intensity.

It begins by correcting the measured scattering from the sample for the sources of background discussed previously, and multiplying the corrected counts by a scaling factor (to remove incidental differences between measurements such as the counting time and sample thickness) that puts the data on an absolute scale of scattering cross section per unit volume. The background-corrected neutron counts, $I_{cor}(q_x,q_y)$, recorded in a 2D-detector pixel are related to the differential macroscopic scattering cross section (the absolute intensity), $d\Sigma(q_x,q_y)/d\Omega$, through the expression

$$I_{cor}\left(q_x,q_y\right) = \phi\ A\ \Delta\Omega\ \varepsilon\ t\ d\ T\ \frac{d\Sigma\left(q_x,q_y\right)}{d\Omega}$$

where:

ϕ = the neutron flux (neutrons/cm^2-sec) at the sample
A = the area of the beam incident on the sample
d = the sample thickness
T = the transmission of the sample
$\Delta\Omega$ = the solid angle subtended by one pixel of the detector
ε = the detector efficiency, and
t = the counting time.

The incidental instrumental factors can be lumped together into one constant, $K = \phi\ A\ \Delta\Omega\ \varepsilon\ t$, and the intrinsic quantity $d\Sigma(q_x,q_y)/d\Omega$, the differential scattering cross section per unit volume, is obtained by scaling the recorded counts

$$\frac{d\Sigma\left(q_x,q_y\right)}{d\Omega} = \frac{I_{cor}\left(q_x,q_y\right)}{KdT}$$

We now go over the specific steps involved in extracting $d\Sigma(q)/d\Omega$ from the raw data. The raw scattered intensity measured from the sample, I_{sam}, and the empty cell, I_{emp}, can be written as

$$I_{sam}\left(q_x,q_y\right) = KdT_{sample+cell}\left[\left(\frac{d\Sigma\left(q_x,q_y\right)}{d\Omega}\right)_{sam} + \left(\frac{d\Sigma\left(q_x,q_y\right)}{d\Omega}\right)_{emp}\right] + I_{bgd}\left(q_x,q_y\right)$$

$$I_{emp}\left(q_x,q_y\right) = KdT_{cell}\left(\frac{d\Sigma\left(q_x,q_y\right)}{d\Omega}\right)_{emp} + I_{bgd}\left(q_x,q_y\right)$$

where $T_{sample+cell}$ and T_{cell} are the measured transmission of the sample (at each temperature) and the empty cell, respectively. From the above, the background corrected scattering, denoted I_{cor}, is given by

$$I_{cor}\left(q_x,q_y\right) = \left[I_{sam}\left(q_x,q_y\right) - I_{bgd}\left(q_x,q_y\right)\right] - \frac{T_{sample+cell}}{T_{cell}}\left[I_{emp}\left(q_x,q_y\right) - I_{bgd}\left(q_x,q_y\right)\right]$$

For simplicity reason, we assume here the neutron flux is stable, and the counting times for sample and sample cell are the same. (In fact, the neutron flux can change with time and depends on reactor stability. This has been considered by monitoring the beam flux change in the beamline. The counting times for sample and sample cell can be different too. A scaling factor based on the relative counting time can be applied in the above equation to take this into consideration.) The corrected counts, I_{cor}, are proportional to the quantity of interest, namely the differential scattering cross section. From the above equations,

$$I_{cor}(q_x, q_y) = KdT_{sample+cell}\left(\frac{d\Sigma(q_x, q_y)}{d\Omega}\right)_{sample}$$

The result of the data correction is a two-dimensional absolute, corrected scattering differential scattering cross section $\left(\frac{d\Sigma(q_x, q_y)}{d\Omega}\right)_{sample}$ as a function of the q-values (corresponding to detector pixels) q_x and q_y.

For isotropic scattered samples, one can take azimuthal average to have the absolute scattering intensity as a function of q only $\frac{d\Sigma(q)}{d\Omega}$

5.2 Examples of reduced data

During our SANS experiment, we will collect the data at different temperatures and sample compositions. Figure 8 shows the reduced data collected in a experiment. You can see that the scattering intensity is very sensitive to the temperature change.

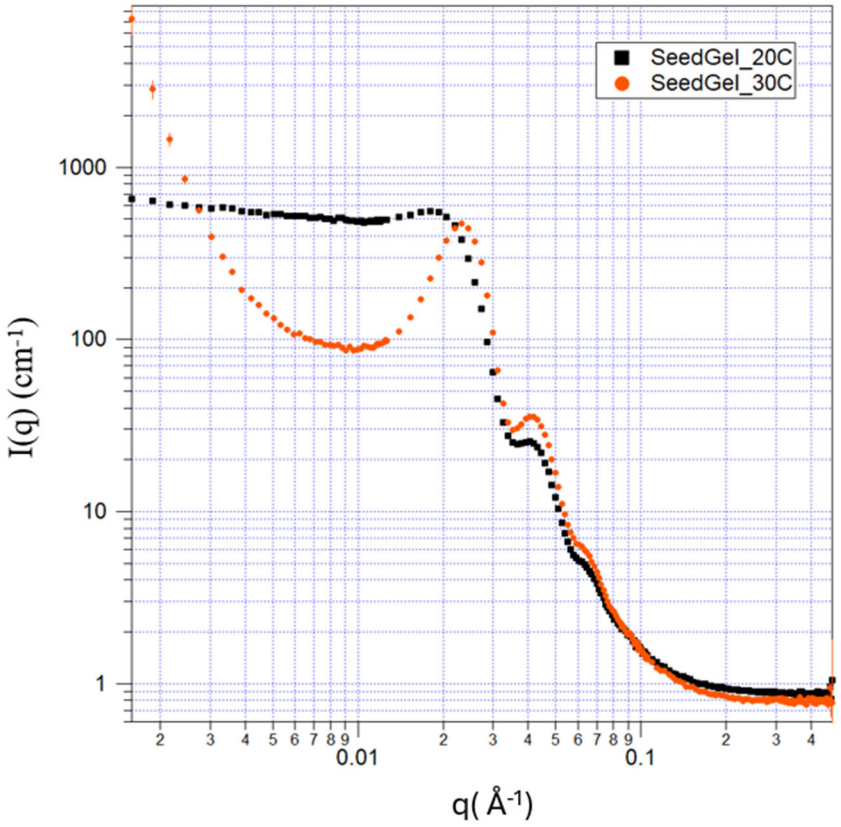

Figure 9. Temperature-dependent SANS data of a SeedGel sample.

The intensity variation with temperature is solely due to the adsorption of CD_4 molecules into the pores because a separate experiment indicates that intensity of empty MCM-41 does not change with temperature in the temperature range being studied.

When temperature decreases from 295 K, the peak intensity first increases gradually and then drops abruptly at certain temperature range, and eventually the intensity increases again.

6. SANS data of a SeedGel sample

The structure of a SeedGel sample is complex. It is best to combine USANS and SANS as USANS can probe the large length scale structure, i.e., the domain size information. On the other hand, SANS can provide the internal structure information of the particle domain due to the packing of nanoparticles with the diameter of about 27 nm.

To prove particles are all packed in the water rich solvent phase, a contrast matching experiment was designed by mixing H_2O and D_2O so that the SLD of water matches to that of silica particles. If all particles are packed inside water rich solvent, the interaction peak at high Q (around 0.23 $Å^{-1}$) is expected to become very small. This is schematically illustrated in Figure 10(a). The SANS data in Figure 10(b) clearly indicate that the peak intensity at around 0.23 becomes very small. This experiment conclusively demonstrated that particles are indeed packed in the water rich phase region in the SeedGel. We will need to calculate the mixing ratio of H_2O and D_2O in order to match the water SLD with that of silica particles.

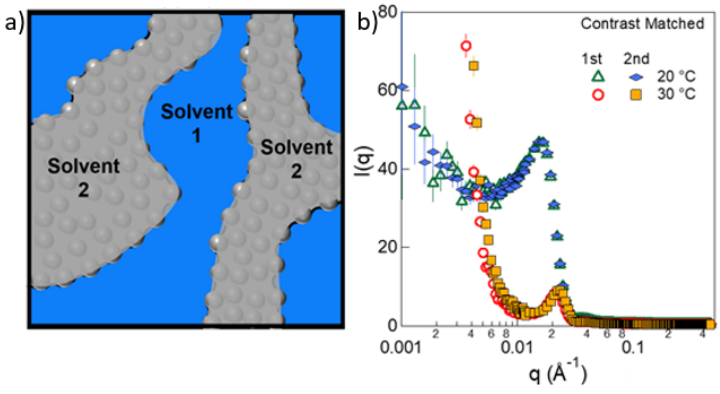

Figure 10. (a) Schematic picture to show that the SLD of solvent in water rich phase is matched to the SLD of silica particles. (b) the SANS data when the water SLD is matched to that of silica particles.

Figure 11 shows the SANS patterns of our sample at different temperatures. The sample was prepared using H_2O. At 20 ºC, the sample is in the liquid state and shows a broad peak that is typical for particles in liquid states. By increasing temperature to about 26 ºC , the sample

becomes a SeedGel as shown by the rheological data in Figure 3. Note that when water SLD is not matched with silica particles, the peak at high Q becomes much stronger in Figure 13.

For the SANS data at Q > 0.01 $Å^{-1}$, the scattering patterns are mainly due to the particles packed inside the particle domain. Usually, the location of the main peak is correlated well with average distance between particles. Once becoming gel, the location of the main peak shifts to a larger Q value, which indicates that the inter-particle distance becomes smaller. This is consistent with the fact that all silica particles are packed inside the particle domain.

Interestingly, after the sample becomes a SeedGel, the scattering pattern does not change too much by further increasing temperatures. Thus, without any data analysis, it shows that the color change is not likely due to the change of particle packing structures inside the particle domain either.

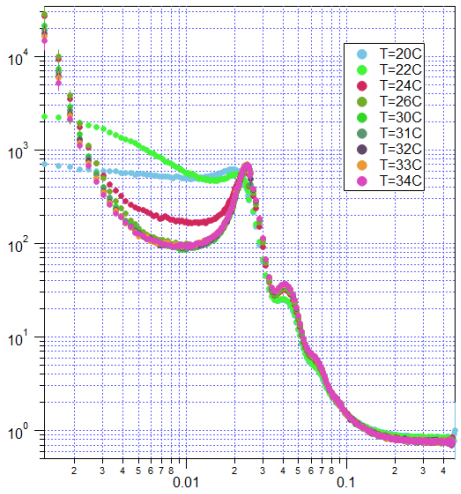

Figure 11 SANS patterns of the sample at liquid and gel states.

7. SANS data analysis

To fit the SANS data at high Q range, one needs to consider both the form factor, P(Q), and the inter-particle structure factor, S(Q), as the particle concentration is high in the particle domain. From the SANS fitting, we can extract the particle volume fraction in the particle domain.

In a liquid system at equilibrium conditions, the relative positions of colloidal particles are governed by the inter-particle potential. Any change of the potential affects the arrangement of colloidal particles in solutions and will be reflected by a corresponding change in the scattering pattern. For a monodisperse hard-sphere system the coherent scattering pattern $I(q)$ can be expressed as

$$I(q) = AP(q)S(q) \qquad (17)$$

where $A = \phi V \Delta\rho^2$, and ϕ, V, and $\Delta\rho$ are the volume fraction of the particles, the particle volume and the scattering length density contrast term respectively; $P(q)$ is the normalized form factor, which is only related with the shape of a particle, and $S(q)$ is the inter-particle structure factor that is related with the inter-particle potential. At dilute concentrations, $S(q) \approx 1$. The scattering pattern of a dilute sample is thus determined by the form factor as $I(q) = AP(q)$. Once we have the information for $P(q)$ at small concentrations, we can extract $S(q)$ at higher concentrations.

$S(q)$ is essentially a measure of the correlation function of the relative positions of the center of mass of particles. If a system is at equilibrium, S(q) can be determined by the inter-particle potential and calculated using statistical mechanical theories. The details of how to calculate S(q) is beyond the scope of this simple lecture (see [11] for details). Because the particles are highly charged, we can model the interaction potential as a screened Coulombic potential. S(Q) for this kind of potential can be calculated to fit the experiment data. The theory originally proposed by Waisman in 1973 [12] was applied to study the charge interaction between colloidal particles by Hayter in 1983.[13] The Hayter_msa method is already implemented in SasView. We will use the SasView to fit the experiment data to obtain the approximate volume fraction of particles in the particle domain.

For a sample at liquid states, at relatively high Q, $S(q) \approx 1$ for even highly concentrated samples.

$$I(q) = \phi V \Delta\rho^2 P(q) \qquad (18)$$

Thus, the high Q data of concentrated solutions are dominated by the form factor. Interestingly, we can observe that there are slight changes of the intensity at high Q. Because the total volume fraction of silica particle is the same and the normalized form factor, P(Q), should remain the same, the only parameter that can affect the scattering pattern in Equation (18) at high Q is the contrast term, $\Delta\rho$, which is the SLD difference between silica particles and the solvent surrounding the particles. Because the SLD of silica particles is expected to be the same at the temperature range, the change of the contrast term can only be due to the change in the solvent SLD. Thus, changing the temperature in the SeedGel can cause the solvent composition change between the particle domains and the solvent domains. It is this solvent exchange between the two domains that introduces the color change of the sample when changing the same temperature.

8. USANS data

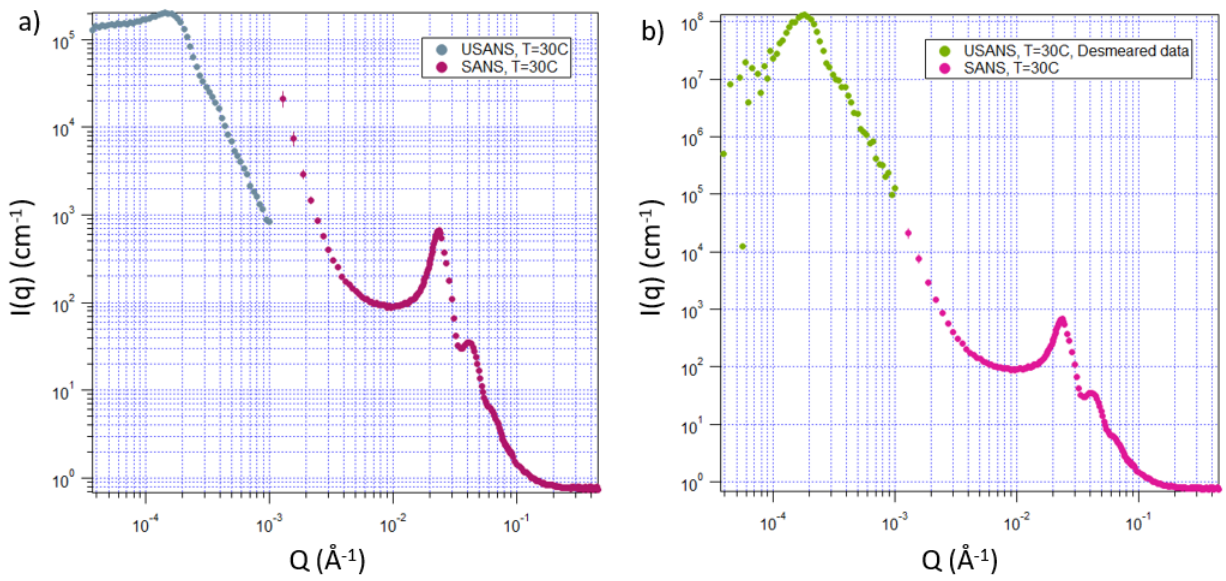

Figure 12. (a) USANS and SANS data for a SeedGel sample. (b) The desmeared USANS data are plotted together with the SANS data.

Figure 12(a) shows the SANS data together with USANS of a SeedGel sample in the same plot. Because USANS data can reach much smaller Q range, it can probe the relative domain size by fitting the UANS data, which is about a couple of micrometers.

The scattering intensity around Q=0.001 $Å^{-1}$ is dramatically different for USANS and SANS data. There is nothing wrong with the data or the measurement. This difference is actually expected due to the difference of the resolution function of the two instruments. USANS has a slit smearing effect due to the instrument design. In comparison, the relative resolution of SANS has much smaller impact on the scattering intensity. Thus, the data from USANS and SANS are expected to be quite different at the same Q range. It is also known that due to the resolution smearing effect of the USANS, the power law decay is also affected by the slit smearing effect.

After desmearing the USANS data to remove the resolution function effect, the results in Figure 12(b) shows that the absolute intensity has a smooth continuation from the USANS Q range to the SANS Q range. Even though desmearing is useful to comparing the data from USANS and SANS, one needs to be aware that there are assumptions used during the desmearing process. To reliably extract the information from USANS data, one is encouraged to use a theoretical model to fit the data in Figure 11(a) by including the resolution function.

Advanced discussion: Why is the solvent exchange responsible for the color change of a SeedGel sample?

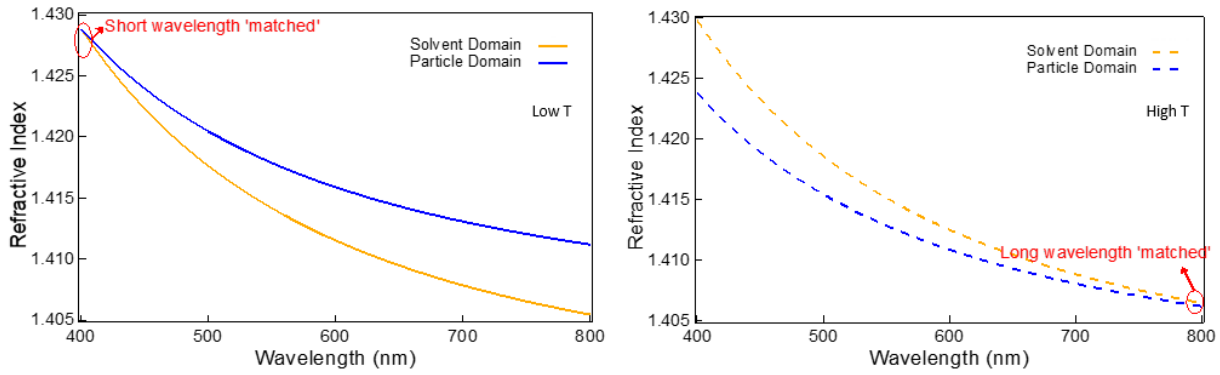

Figure 13. The calculated refractive index of the particle and solvent domains as a function of the wavelength.

The average refractive index of the two domains depends on the wavelength.[3] In Figure 13, the solid lines show the calculated refractive index of the particle domain (solid blue curve) and the solvent domain (solid orange curve) at low temperature for the SeedGel. It shows that the two lines match only at shorter wavelength. Thus, light with longer wavelength will be scattered away by the bicontinuous structures. Because red and yellow colors have longer wavelength, the structure color of a SeedGel sample shows a yellowish color at low temperature. However, when increasing the temperature, there is an exchange of solvent molecules between the two domains. The particle domain loses lutidine to the solvent domain and gains water from the solvent domain. Because the refractive index of water is smaller than that of lutidine, this solvent exchange decreases the average refractive index of particle domain and increases the average refractive index of the solvent domain. As a result, when increasing the temperature, the refractive index of the particle domains moves down in Figure 14 to become dashed blue curve while the refractive index of the solvent domain moves up from solid orange cure to dashed orange curve. Because of these shifts, the refractive index of the solvent and particle domain only matches at longer wavelength. Any light with longer wavelength will not be scattered and pass through the sample. The light with shorter wavelength are scattered at high temperature. Because light with shorter wavelength tends to be blueish, the SeedGel sample shows blue color at high temperature. Because the solvent composition exchange is thermoreversible. The color change of a SeedGel is thus also thermoreversible. The physics mechanism of this phenomenon is called the Christiansen effect. The details are discussed in the Ref[2].

9. Summary

Through this experiment you shall learn the following concepts and understand how to apply them to gain useful information from your measurements:

Objectives of the Experiment:

- Get familiar with the SANS technique, how to optimize a sample for SANS and extract useful information from SANS data.
- Calculate the H_2O and D_2O ratio needed to match the water SLD with that of silica particles.
- Determine the form factor using a dilute sample.
- Familiar with the structure factor by fitting SANS data of concentrated samples.

Scattering theories:

1) Contrast matching experiment design.
2) What is the form factor, P(q)
3) What is the inter-particle structure factor, S(q)
4) The scattering contrast between colloidal particle and solvent
5) For a monodisperse system, $I(q) = AP(q)S(q)$
6) The colloidal interaction information can be extracted by fitting I(q)

References

[1] Y. Xi, R. Lankone, L. Sung, and Y. Liu, NATURE COMMUNICATIONS **12**, 910 (2021).
[2] Y. Xi, F. Zhang, Y. Ma, V. Prabhu, and Y. Liu, NATURE COMMUNICATIONS **13**, 3619 (2022).
[3] M. FISHER and P. GENNES, Comptes Rendus Hebdomadaires Des Seances De L Academie Des Sciences Serie B **287**, 207 (1978).
[4] T. BURKHARDT and E. EISENRIEGLER, Physical Review Letters **74**, 3189 (1995).
[5] D. BEYSENS and D. ESTEVE, Physical Review Letters **54**, 2123 (1985).
[6] E. Herzig, K. White, A. Schofield, W. Poon, and P. Clegg, Nature Materials **6**, 966 (2007).
[7] K. Stratford, R. Adhikari, I. Pagonabarraga, J. Desplat, and M. Cates, Science **309**, 2198 (2005).
[8] C. GRATTONI, R. DAWE, C. SEAH, and J. GRAY, Journal of Chemical and Engineering Data **38**, 516 (1993).
[9] C. E. Bertrand, P. D. Godfrin, and Y. Liu, Journal of Chemical Physics **143**, 084704 (2015).
[10] Y. Xi *et al.*, Soft Matter **19**, 233 (2023).
[11] C. Caccamo, Physics Reports-Review Section of Physics Letters **274**, 1 (1996).
[12] E. WAISMAN, Molecular Physics **25**, 45 (1973).
[13] J. HAYTER and J. PENFOLD, Molecular Physics **42**, 109 (1981).